

^{87}Sr NMR of phase transitions in $\text{SrTi}^{16}\text{O}_3$ and $\text{SrTi}^{18}\text{O}_3$ Valentin V. Laguta,¹ Robert Blinc,² Mitsuru Itoh,³ Janez Seliger,² and Boštjan Zalar²¹*Institute for Problems of Material Sciences, Ukrainian Academy of Sciences, Krjijanovskogo 3, 03142 Kiev, Ukraine*²*J. Stefan Institute, Jamova 39, 1000 Ljubljana, Slovenia*³*Materials and Structures Laboratory, Tokyo Institute of Technology, 4259 Nagatsuta, Midori, Yokohama, 226-8503, Japan*

(Received 29 August 2005; published 13 December 2005)

^{87}Sr quadrupole perturbed NMR data of SrTiO_3 show that local symmetry breaking takes place also at the A site of the ABO_3 perovskite lattice in the cubic phase and not only at the B site as observed before. This is true for $\text{SrTi}^{16}\text{O}_3$ (STO-16) and $\text{SrTi}^{18}\text{O}_3$ (STO-18). The onset of the antiferrodistortive transition around $T_a = 105$ K is accompanied by a huge splitting of the ^{87}Sr NMR line due to formation of macroscopic 90° domains and an anomalous shortening of the spin-spin relaxation time T_2 of the quadrupole satellite transitions which persist in the tetragonal phase down to 30 K. This shows the presence of very low frequency fluctuations of the phase transition order parameter. Rhombohedral polar clusters appear in the tetragonal matrix both in STO-16 and STO-18 below 70 K and percolate in STO-18 below $T \approx 24$ K leading to an inhomogeneous ferroelectric state. This is also supported by measurements of the field cooled ^{87}Sr NMR spectra.

DOI: [10.1103/PhysRevB.72.214117](https://doi.org/10.1103/PhysRevB.72.214117)

PACS number(s): 77.84.Dy, 76.30.Fc, 76.60.-k, 77.80.Bh

I. INTRODUCTION

SrTiO_3 (abbreviated as STO-16) is considered to be a classical displacive system¹ where the low temperature ferroelectric phase is suppressed by zero point quantum fluctuations² of the soft mode. The zero temperature displacement of the “ferroelectric” titanium ion, $\Delta z(0)$, is assumed to be smaller than the mean zero point fluctuation amplitude $\sqrt{\langle \delta z^2 \rangle}$ of this ion. The discovery of Itoh *et al.*³ of ferroelectricity in ^{18}O isotope enriched $\text{SrTi}^{18}\text{O}_3$ (STO-18) around $T_c = 24$ K seems to support this assumption. The larger mass of ^{18}O reduces zero point fluctuations and allows for the condensation of the polar soft mode at a finite temperature if the ^{18}O concentration x exceeds a critical value x_c . The symmetry of the low temperature ferroelectric phase is not yet established but is not tetragonal.

Both STO-16 and STO-18 undergo an antiferrodistortive transition⁴ at $T_a = 105$ K which is connected with a condensation of a nonpolar soft mode at the Brillouin zone boundary.^{1,4} This antiferrodistortive transition from the cubic $Pm\bar{3}m$ phase to the tetragonal $I4/mcm$ phase is accompanied by alternating rotations of the corner sharing oxygen octahedra.⁴ The rotation angle $\phi(T)$ is the order parameter of this structural phase transition. Müller *et al.*⁵ found a phase transitionlike anomaly in the temperature dependence of $\phi(T)$ in STO-16 near 38 K. The deviation of the rotation angle from the value predicted by the microscopic theory of Pytte and Feder⁶ could be interpreted as being proportional to the square of an additional order parameter which varies with temperature as $\Delta\phi(0)(T - T_q)^{1/2}$ with $T_q = 38$ K and $\Delta\phi(0) \approx 0.08^\circ$. This phenomenon was tentatively discussed as a possible transition to a novel coherent quantum state.⁵ However, no microscopic symmetry change has been detected.

Recent Ti NMR data^{7,8} have shown the existence of dynamic disorder of the Ti ions in the cubic phase in a number of perovskites. The Ti ions do not occupy the central ideal

perovskite position in the oxygen octahedra but are off-center. This is revealed by the nonzero quadrupole coupling and nonzero electric field gradient (EFG) tensor at the Ti sites in STO-16, STO-18, and BaTiO_3 .^{7,8} The cubic symmetry of the high temperature phase is thus locally broken. The macroscopic cubic symmetry is the result of time and space averaging. The Ti motion between different off-center sites is accompanied by different dynamic distortions of the locally tetragonal unit cells.⁸ The phase transition mechanism has thus both order-disorder and displacive components in BaTiO_3 as well as in STO-16 and STO-18.

Since ^{87}Sr NMR is considerably more sensitive to small rotations and distortions of the oxygen octahedra than Ti NMR, we decided to study the low temperature transition in STO-18 and STO-16 by quadrupole perturbed ^{87}Sr NMR. In our preliminary NMR study⁹ we have already shown that the elusive ferroelectric transition in STO-18 is indeed connected with local symmetry lowering and implies the existence of an order-disorder component in addition to the displacive soft mode one. In the present paper using ^{87}Sr NMR and Fe^{3+} electron spin resonance (ESR) we have continued to study this topic to get further insight into the mechanism leading to the ferroelectric transition in STO-18 as well as additional information on the anomaly at $T_q = 38$ K in STO-16 and the antiferrodistortive cubic-tetragonal transition at $T_a = 105$ K. In particular, our zero field cooled and field cooled ^{87}Sr NMR measurements show that the low-symmetry clusters, which appear in the tetragonal matrix of SrTiO_3 , are indeed rhombohedral polar clusters. They percolate in STO-18 below $T \approx 24$ K leading to an inhomogeneous ferroelectric state.

II. EXPERIMENT

The STO-18 measurements were performed on a sample composed of 6 to 7 single crystal plates with dimensions $7 \times 3 \times 0.3$ mm³ and oriented with two edges parallel to the

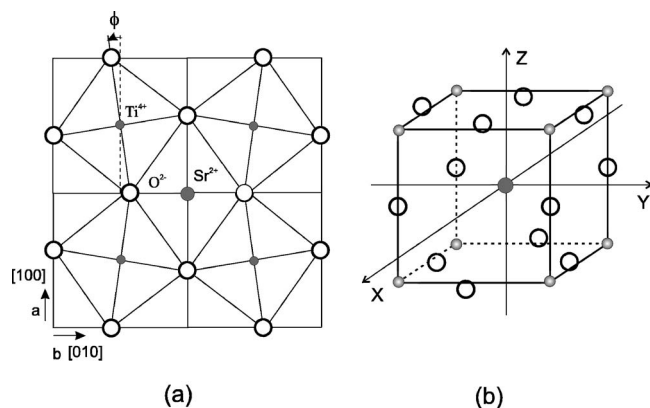


FIG. 1. (a) Part of the SrTiO₃ lattice with oxygen octahedra distortions in the *a-b* plane. (b) Displacements from the cubic lattice along the *c* axis leading to tetragonality.

{110} planes as well as on one plate with dimensions $8 \times 6 \times 0.3$ mm³ cut in the (111) plane. The isotopic exchange method has been described by Itoh and co-workers,³ and the ¹⁸O enrichment was about 95%, with $T_c \approx 24$ K. The reference STO-16 measurements were performed on a $7 \times 4 \times 4$ mm³ sample with two edges parallel to the {110} planes.

A two $\pi/2$ pulse, four phase (*xx, xy, x-x, x-y*) “exorcycle” phase sequence¹⁰ was used to observe the ⁸⁷Sr ($I=9/2$) central $1/2 \leftrightarrow -1/2$ and satellite transitions in a magnetic field $B=9.2$ T corresponding to a Larmor frequency of 16.471 MHz. The length of the $\pi/2$ pulse was typically 3 to 4 μ s. Below 90 K the spin-spin relaxation time T_2 became too short to apply the spin echo sequence and the free induction decay signal was used. The spin-lattice relaxation time T_1 , on the other hand, is long and varies from several seconds at room temperature to up to 1 h at 14 K. The huge difference between T_1 and T_2 found by us shows the presence of very low frequency dynamics at $T < 105$ K. Since the low frequency dispersion was not observed in the dielectric data, it could indicate the presence of nonpolar fluctuations.

In order to check the domain structure of the crystals in the tetragonal phase and measure the rotation angle $\phi(T)$ of the oxygen octahedron in both STO-16 and STO-18 we used Fe³⁺ ESR at 9.2 to 9.3 GHz. The STO crystals were not specially doped by iron. The Fe³⁺ ions (~ 10 – 20 ppm) were present in our samples as a background impurity.

III. THE ELECTRIC FIELD GRADIENT (EFG) TENSOR AT THE Sr SITES

The EFG tensor at the Sr sites is zero by symmetry in the ideal perovskite cubic lattice. Due to the rotation of the oxygen octahedra in the tetragonal phase below $T_a=105$ K the EFG tensor is expected to become nonzero.

The projection of one layer of oxygen octahedra on the *a-b* plane is shown in Figs. 1(a) and 1(b) for the tetragonal phase of STO. As it can be seen the Sr-O distances are markedly reduced from the $\sqrt{2}/2c$ value in the cubic phase due to the rotational displacement of the TiO₆ octahedra resulting in a nonzero EFG at the Sr sites as expected.

Assuming that the cubic symmetry at the Sr sites is broken solely due to rotations of the surrounding oxygen octahedra^{4,5} and taking into account only the charges of the 12 closest oxygen ions (the Ti ions are more distant and located at nearby cubic positions), one finds in the point charge approximation the following expressions for the components of the EFG tensor at the Sr sites:

$$V_{xx} = V_{yy} = (1 - \gamma_\infty) 63 \sqrt{2} e \phi^2 / c^3, \quad (1a)$$

$$V_{zz} = -(1 - \gamma_\infty) 126 \sqrt{2} e \phi^2 / c^3, \quad (1b)$$

$$V_{ij} = 0, \quad i, j = x, y, z. \quad (1c)$$

Here the *x*, *y*, *z* axes are parallel to the unit cell edges. *c* is the lattice constant, γ_∞ is the Sr antishielding factor (we assume that $1 - \gamma_\infty$ is 14, a bit smaller than that for ⁹³Nb in KNbO₃, Ref. 11), and ϕ is the nominal rotation angle (in radians) of the oxygen octahedra. We also took into account the relation between the lattice constants $c/a = 1/\cos \phi$. The extension of the summation to a larger number of oxygen ions shows that the EFG remains proportional to the square of the order parameter (a similar calculation was performed, for example, for KMnF₃, Ref. 12) and its value oscillates within 50% of the value given above. In Eqs. (1a) and (1b) we have also omitted the contribution from the electronic polarization. However, this is not important, because the proportionality coefficient between V_{ii} and ϕ^2 will be obtained from Fe³⁺ ESR data. We shall note that the above “oxygen rotation” point charge model properly accounts for the observed cubic-to-tetragonal symmetry breaking, except possibly for the quantitative values of the proportionality constants of Eqs. (1a)–(1c). In order to refine this, the more distant ions and/or density functional modeling should have been employed. Such a calculation is, however, outside the scope of this paper.

Within the same approximation, i.e., taking into account only the first shell of the oxygen ions the EFG components at the central Ti site due to the tetragonal distortion are given by

$$V_{zz} = -(1 - \tilde{\gamma}_\infty) [1 - (c/a)^3] 8e/c^3, \quad (2a)$$

$$V_{xx} = V_{yy} = -V_{zz}/2. \quad (2b)$$

Here $\tilde{\gamma}_\infty$ is the Ti antishielding factor. Within a good approximation we can take for it the value $1 - \gamma_\infty \approx 10$ obtained in BaTiO₃.¹³ As in the case of the Sr site the sum over more shells of ions leads to oscillations of the EFG value within 50%. The important point is that a comparison of expressions (1a)–(1c), (2a), and (2b) shows that V_{zz} at the Ti site is more than ten times smaller than at the Sr site even for equal values of their antishielding factors. This is due to the fact that the tetragonal deformation of the unit cell is very small as $(c/a) - 1 = 8.2 \times 10^{-4}$ even at 4.2 K and the oxygen octahedron remains undistorted under the antiferrodistortive structural phase transition at $T_a=105$ K. Therefore ⁸⁷Sr NMR should be much more sensitive to the rotations of the oxygen octahedra than Ti NMR. In addition the Ti ions are

off-center so that there is a second contribution to the V_{zz} at the Ti sites.

It may also be worthwhile to evaluate the EFG tensor for a small displacement of the Sr or Ti ion from its cubic site in the undistorted perovskite lattice. The electric potential V in the vicinity of a cubic site can be developed in a Taylor series in powers of the displacements

$$V = A(x^2 + y^2 + z^2) + B(x^4 + y^4 + z^4) + C(x^2y^2 + x^2z^2 + y^2z^2) + \dots, \quad (3)$$

where the coefficients A , B , and C depend on the distance to the surrounding ligands, their charge, and local symmetry.

From the Laplace equation $\Delta V = 6A + (12B + 4C)(x^2 + y^2 + z^2) = 0$ we find $A = 0$ and $C = -3B$. The x , y , and z directions point along the cubic unit cell edges. Let us now introduce $x' = (x + y)/\sqrt{2}$ and $y' = (x - y)/\sqrt{2}$. The x' axis now points along the $[110]$ direction. In the new $x'y'z'$ coordinate system the potential (3) becomes

$$V = 1/4B[(-x'^4 - y'^4 + 4z'^4) - 6(2z'^2x'^2 + 2z'^2y'^2 - 3x'^2y'^2)]. \quad (4)$$

Let us now assume that the Sr or Ti displacements from the cubic site lie in the $x'z'$ plane and can be expressed as $z' = z = d \cos \vartheta$, $x' = d \sin \vartheta$. The components of the EFG tensor at the displaced site can then be rewritten as

$$V_{x'x'} = 3B'd^2(-1 - \cos^2 \vartheta), \quad (5a)$$

$$V_{zz} = 6B'd^2(3 \cos^2 \vartheta - 1), \quad (5b)$$

$$V_{y'y'} = 3B'd^2(3 - 5 \cos^2 \vartheta), \quad (5c)$$

$$V_{x'z'} = -12B'd^2 \sin \vartheta \cos \vartheta, \quad (5d)$$

where $B' = (1 - \gamma_\infty)B$.

The EFG tensor eigenvalues are

$$V_{11} = V_{y'y'} = 3B'd^2(3 - 5 \cos^2 \vartheta), \quad (6a)$$

$$V_{22}, V_{33} = 3/2B'd^2[(5 \cos^2 \vartheta - 3) \pm \sqrt{1 + 50 \cos^2 \vartheta - 15 \cos^4 \vartheta}]. \quad (6b)$$

Introducing $V_{kk} = 3B'd^2\lambda_{kk}$ we find for different displacement directions, e.g., for

$$\vartheta = 0: \quad \lambda_{kk} = 4, -2, -2; \quad \eta = 0, \quad (7a)$$

$$\vartheta = \vartheta_M = 54.7^\circ: \quad \lambda_{kk} = -8/3, 4/3, 4/3; \quad \eta = 0, \quad (7b)$$

$$\vartheta = 90^\circ: \quad \lambda_{kk} = 3, -1/2, -5/2; \quad \eta = 0.67, \quad (7c)$$

$$\vartheta = 39^\circ: \quad \lambda_{kk} = \pm \sqrt{128/5}, 0; \quad \eta = 1. \quad (7d)$$

The EFG tensor is thus in all above cases proportional to the square of the displacement d from the cubic site.

In the general case the EFG tensor is the sum of contributions (7) and (1) or (2) for the Sr and Ti sites, respectively. In particular one can notice that for the off-center Ti ions in

the tetragonal phase the two contributions to EFG have opposite signs whereas for the Sr sites these two contributions are of the same sign. For example, in the case of Ti displacement along the $[001]$ axis the EFG has the simple form:

$$V_{zz} \approx (1 - \gamma_\infty) \frac{8e}{c^3} \left[\left\{ 1 - \left(\frac{c}{a} \right)^3 \right\} + \frac{6}{c^2} d^2 \right]. \quad (8)$$

Therefore the resulting changes in the EFG components at Ti sites can be very small at $T \leq T_a$ and the corresponding changes in the NMR spectra are hardly or not at all detectable.

The first-order quadrupole induced frequency shift $\Delta\nu_m = \nu_{m-1 \leftrightarrow m} - \nu_L$ of the $m-1 \leftrightarrow m$ NMR transition is given by¹⁴

$$\Delta\nu_m^{(1)} = -\nu_q(m-1/2)/2(3 \cos^2 \Theta - 1 + \eta \sin^2 \Theta \cos 2\Phi) \quad (9)$$

where $\nu_q = 3K/[2I(2I-1)]$ is the quadrupole frequency. $K = e^2qQ/h$ is the quadrupole coupling constant which is proportional to the largest eigenvalue $V_{zz} = eq$ of the EFG tensor whereas η is the asymmetry parameter which measures the biaxiality. Θ and Φ are the tilt and azimuth angles of the direction of the external magnetic field \mathbf{B} with respect to the xyz EFG tensor eigenframe.

The EFG tensor at the Sr site resulting from the alternating rotations of the oxygen octahedra at and below T_a is cylindrically symmetric, so that the asymmetry parameter $\eta = (V_{xx} - V_{yy})/V_{zz}$ equals zero. The largest principal axis of the EFG tensor is parallel to the tetragonal c axis of the given domain.

The $1/2 \leftrightarrow -1/2$ NMR transition is not shifted in first order. The second-order quadrupole shift of this transition is for $\eta = 0$ given by¹⁴

$$\Delta\nu_{1/2 \leftrightarrow -1/2}^{(2)} = -\frac{\nu_q^2}{16\nu_L}(a-3/4)(1 - \cos^2 \Theta)(9 \cos^2 \Theta - 1) \quad (10)$$

where $a = I(I+1)$. For $\mathbf{B} \parallel [111]$ the largest principal axis V_{zz} of all three $\langle 100 \rangle$ type domains make the "magic" angle $\Theta_m = 54.7^\circ$ with the direction of the magnetic field \mathbf{B} so that the corresponding NMR lines will coincide.

IV. RESULTS AND THEIR INTERPRETATION

A. Fe³⁺ ESR characterization

All samples investigated showed ESR spectra of both the Fe³⁺ charge-noncompensated and Fe³⁺-V_O charge compensated paramagnetic centers (V_O denotes an oxygen vacancy). Fe³⁺ spectra are well studied in SrTiO₃ (see, for example, Refs. 4 and 15) and usually used for the direct determination of the order parameter $\phi(T)$ of the 105 K phase transition. This is true because in the tetragonal phase the orthogonal system of axes, which defines the fourth-degree crystal-field cubic terms of Fe³⁺ spin Hamiltonian and is directed towards the oxygens around the Fe³⁺, is rotated with respect to the crystalline axes by an angle ϕ [Fig. 1(a)]. Therefore in the crystalline axes frame the spin Hamiltonian has additional terms containing the angle ϕ .¹⁶

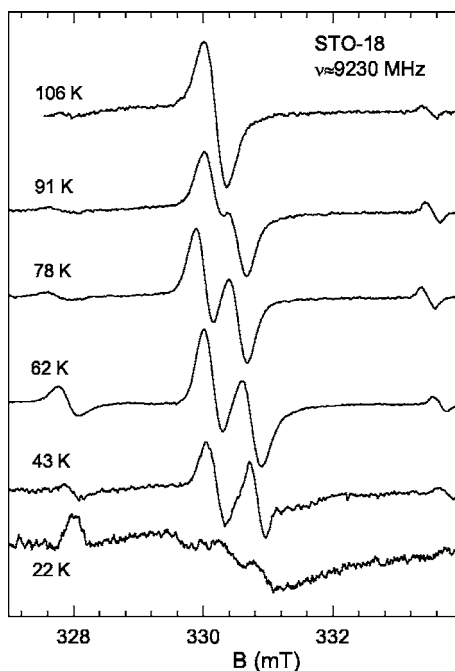


FIG. 2. Temperature dependence of $\text{Fe}^{3+} 1/2 \leftrightarrow -1/2$ transition in STO-18 measured at $\theta=90^\circ$ and $\varphi=10^\circ$.

$$\mathbf{H} = g\mathbf{B}\mathbf{S} + \frac{1}{3}b_2^0O_2^0 + \frac{1}{60}b_4^0O_4^0 + \frac{1}{60}(b_4^4O_4^4 + c_4^4\Omega_4^4), \quad (11)$$

Here $g=2.004$, $S=5/2$, b_2^0 is the tetragonal component of the crystal field which describes the tetragonal distortion of the lattice whereas b_4^0, b_4^4, c_4^4 are the fourth-order cubic terms of the crystal field. The spin operators O_2^0, O_4^4, Ω_4^4 are defined, for example, in Ref. 17.

In the cubic phase b_2^0 and c_4^4 are zero. In the tetragonal phase b_2^0, b_4^4 , and c_4^4 are temperature-dependent, where

$$b_4^4 = b_4^4(\phi=0)\cos 4(\varphi \pm \phi),$$

$$c_4^4 = -b_4^4(\phi=0)\sin 4(\varphi \pm \phi). \quad (12)$$

Here φ is the azimuthal angle of \mathbf{B} and ϕ is the rotation angle of the TiO_6 octahedron. The largest crystal field term in Eq. (11) is $b_4^4 \approx 550 \times 10^{-4} \text{ cm}^{-1}$, while b_4^0 is relatively small ($\approx 110 \times 10^{-4} \text{ cm}^{-1}$) and practically temperature-independent. Due to the multipliers $\cos 4(\varphi \pm \phi)$ and $\sin 4(\varphi \pm \phi)$ in the fourth-degree crystal-field terms each of the ESR transitions splits into two components at $T < T_a$. The splitting is large even for the $\pm 1/2$ central transition. This allows the determination of the angle ϕ with an accuracy around 0.1° , assuming that the above model based on the work of Müller *et al.* is valid.^{4,5} As an example, such a splitting of the ESR line measured in a monodomain STO-18 sample is shown in Fig. 2 for $\theta=90^\circ$ ($\mathbf{B} \perp \mathbf{c}$), $\varphi=10^\circ$. The experimental spectra were simulated using numerical diagonalization of the spin Hamiltonian (11)¹⁸ that allowed us to obtain the temperature dependence of both the b_2^0 and $b_4^4(c_4^4)$ parameters. The temperature dependence of the angle ϕ calculated with the help of relation (12) is presented in Fig. 3. The measurements were performed up to 5 K for STO-16, while for STO-18 this was hardly possible below 40 K due

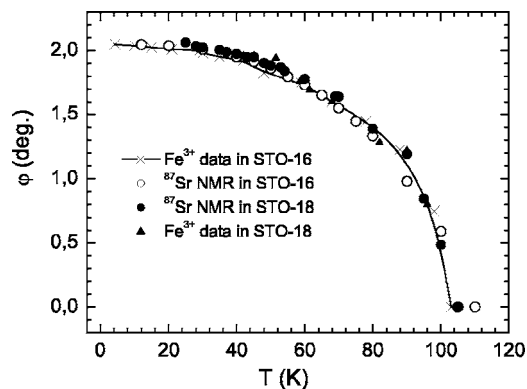


FIG. 3. Temperature dependence of the nominal rotation angle ϕ of the oxygen octahedra [Eqs. (1) and (12)] at $T < T_a = 105$ K as derived from the point charge model (NMR data) and the model of Müller *et al.* (Refs. 4 and 5) (EPR data).

to the very high value of the dielectric constant of STO-18 at these temperatures. It should be stressed that for STO-16 the $\phi(T)$ values determined by us coincide with those from the literature.⁴ The data presented in Fig. 3 show that at least to $\sim 35\text{--}40$ K the temperature variation of the rotational order parameter in STO-18 is completely analogous to the one in STO-16. It should be mentioned that at $T < 30$ K the STO-18 Fe^{3+} EPR spectra become nonaxially symmetric. However, this nonaxiality could not be analyzed at all because of the low intensity of the spectrum. A glasslike broadening also seems to take place at $T=22$ K (Fig. 2).

B. ^{87}Sr NMR spectra and spin-spin relaxation in the cubic phase

The ^{87}Sr NMR spectra were measured at $\mathbf{B} \parallel [100]$, $\mathbf{B} \parallel [110]$, and $\mathbf{B} \parallel [111]$. A representative ^{87}Sr spectrum in the paraelectric phase ($T > T_a \approx 105$ K) is shown in Fig. 4(a). In this phase the spectrum consists of a sharp central line sitting on a broad background, in complete analogy to the spectra of ^{47}Ti and ^{49}Ti in BaTiO_3 , STO-16, and STO-18.⁸ The broad background persists down to the cubic-tetragonal transition temperature $T_a=105$ K. The width of the background component strongly increases and, respectively, its intensity decreases when the temperature approaches T_a . The background component completely disappears below T_a , where well resolved first-order ^{87}Sr quadrupole satellites appear [Fig. 4(b)]. Simultaneously, the central line is split at a general orientation of the crystal in the magnetic field into three lines, corresponding to three 90° tetragonal domains. The splitting exhibits a strong temperature dependence, as it is shown in Fig. 5(a) for $\mathbf{B} \parallel [110]$, reflecting the increase of the rotation angle ϕ of oxygen octahedra with decreasing temperature. The results for STO-16 are qualitatively the same as in STO-18. Evidently, the broad background in the ^{87}Sr NMR spectra is due to unresolved $\pm 1/2 \leftrightarrow \pm 3/2$, $\pm 3/2 \leftrightarrow \pm 5/2, \dots$ quadrupole satellite transitions. The existence of satellites demonstrates the presence of a nonzero EFG tensor at the Sr sites and thus the local breaking of the O_h cubic symmetry at the Sr sites even at $T > T_a$. This is analogous to what we have found for the Ti sites.⁸

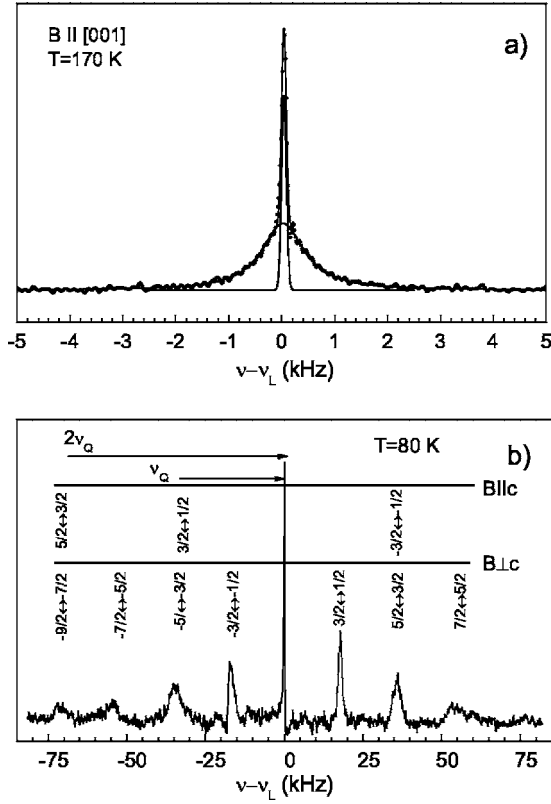


FIG. 4. (a) ^{87}Sr NMR spectrum of STO-18 at $\mathbf{B}||[001]$ and 170 K. The spectrum can be decomposed into a sharp central $1/2 \leftrightarrow -1/2$ Gaussian line and a broad Lorentzian representing the motionally narrowed satellite background. (b) Central line and resolved ^{87}Sr quadrupole satellites in the tetragonal phase of STO-18 at $\mathbf{B}||[001]$ and 80 K. The spectrum consists of contributions from three different tetragonal domains, the first two with the symmetry axes $[100]$ and $[010]$, respectively, perpendicular to \mathbf{B} , and the third one with the symmetry axis $[001]$ along \mathbf{B} .

In order to understand the origin of the nonzero EFG tensor in the cubic phase we performed measurements of the temperature dependence of the spin-spin relaxation time T_2 . This is related in the case of high spin nuclei to the spectral densities of the EFG tensor fluctuations $J(\omega)$ at zero (i.e., very low) frequency, at the Larmor frequency ω_L , and at twice the Larmor frequency $2\omega_L$ (Ref. 14):

$$\frac{1}{T_2} = K[C_0J(0) + C_1J(\omega_L) + C_2(2\omega_L)]. \quad (13)$$

The important point is that $C_0=0$ for the $1/2 \leftrightarrow -1/2$ transition so that $J(0)$ does not contribute to the T_2 of the central transition, whereas $C_0 \neq 0$ for other transitions.¹⁴ Low frequency motions thus do contribute to the T_2 of the satellites. The experimental magnetization decay curve measured at ω_L and 170 K is shown in Fig. 6. A double-exponential decay is found as there are contributions from the central transition (T_{2c}) and the satellite background (T_{2s}). This is so as the central line ‘‘sits’’ on the satellite background. The magnetization decay measured only for satellites exhibits a single-exponential decay characterized by $T_{2s}=0.6$ ms. The tem-

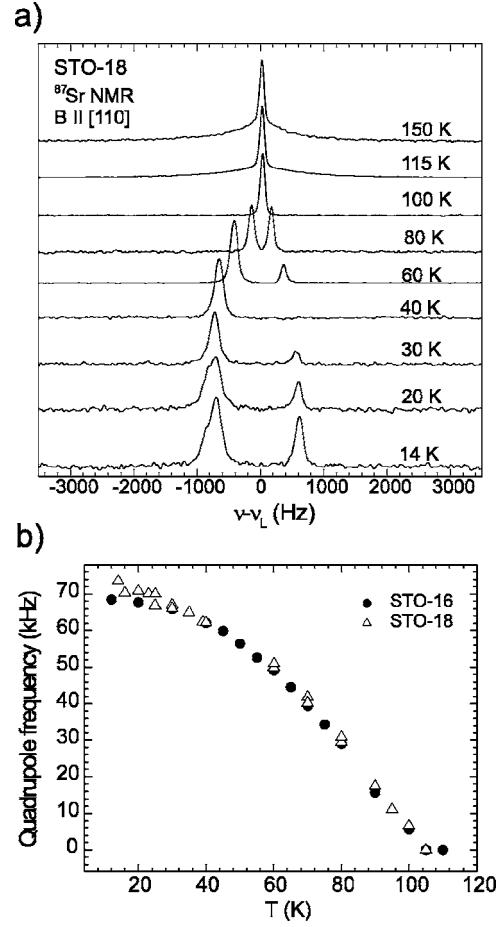


FIG. 5. (a) Temperature dependence of the ^{87}Sr $1/2 \leftrightarrow -1/2$ NMR spectra in the cubic and the tetragonal phases of STO-18 for $\mathbf{B}||[110]$. (b) Temperature dependence of the ^{87}Sr quadrupole frequency ν_q in STO-16 and STO-18. The experimental temperature dependence of ν_q is obtained concurrently with the experimental temperature dependence of the nominal rotation angle ϕ (Fig. 3) by fitting Eq. (10) with $\nu_q(V_{ij}(\phi))$ and $\eta=0$ to the experimental second-order ^{87}Sr $1/2 \leftrightarrow -1/2$ NMR frequency shift.

perature dependence of T_2 for satellites is shown in Fig. 6. The satellite T_2 decreases strongly on approaching the cubic-tetragonal antiferrodistortive transition in STO-16 as well as in STO-18. This means that the rotational fluctuations of the oxygen octahedra contain a strong low frequency component $J(0)$ which increases as $T \rightarrow T_c$. It is interesting to note that T_2 remains short (<0.15 ms—the limit of our measurements) down to about 30 K where the ferroelectric transition in STO-18 takes place. The T_2 value for the central transition is on the other hand practically temperature-independent.

In Fig. 6 we also show the temperature dependence of the inverse value of the full width at half the maximum (FWHM) of the satellite background, which is related to T_2 via

$$\frac{1}{\pi\text{FWHM}} = T_2^*. \quad (14)$$

Here $1/T_2^* = 1/T_2 + 1/T_2^{\text{inh}}$ and T_2^{inh} measures the contribution of the inhomogeneous broadening to the NMR line. Compar-

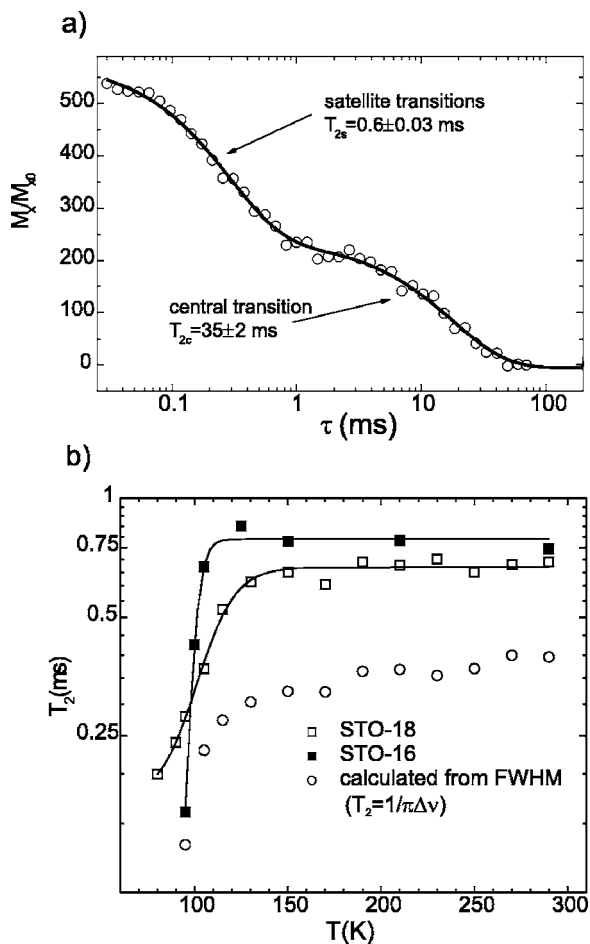


FIG. 6. (a) Two-exponential transverse magnetization decay in STO. (b) Temperature dependence of the satellite T_2 in STO-18 and STO-16 as compared to the FWHM of the ^{87}Sr line. The T_2 of the central transition is long and temperature-independent.

ing the two measured values $1/T_2$ and π FWHM, one can see that the homogeneous contribution $\text{FWHM}_{\text{hom}} = (\pi T_2)^{-1}$ to the measured linewidth is approximately 50% at $T \geq 150$ K but completely dominates at temperatures close to T_a . This means that the observed unresolved satellite background is a motionally averaged spectrum. In this case the theory of destruction of a fine structure of resonance lines through a fast motion¹⁴ predicts a Lorentzian line shape for each $M-1 \leftrightarrow M$ satellite transition, centered at ν_L , with

$$\text{FWHM}_{\text{hom},M} = (\pi T_{2,M})^{-1} = \frac{M_{2,M}(\vartheta, \varphi)}{N\pi W_{\text{exch}}}, \quad (15)$$

where $M_{2,M}(\vartheta, \varphi) = \nu_q^2 [(2M-1)^2/8] M_2(\vartheta, \varphi)$ is the rigid-lattice second moment that would be observed in the case of frozen-in flipping dynamics. ν_q is the quadrupole frequency corresponding to each of the N chemically equivalent sites among which a fast exchange is presumably performed and W_{exch} is the probability per unit time for an exchange between two sites. $M_2(\vartheta, \varphi)$ is the dimensionless second moment of the satellite background which depends on the symmetry group of the N -site potential and on the orientation of

the crystal in the magnetic field, given by the angles ϑ and φ .⁸

For nuclear spins $I > 1/2$ the cumulative motionally averaged satellite spectrum is a transition probability-weighted superposition of individual satellite contributions with M -dependent linewidths $\text{FWHM}_{\text{hom},M}$. In the time domain this leads, respectively, to a multiexponential decay of the transverse magnetization M_x :

$$\frac{M_x(\tau)}{M_x(0)} = \frac{\sum_{M=-I+1}^I J(M,I) e^{-2\tau/T_{2,M}}}{\sum_{M=-I+1}^I J(M,I)}. \quad (16)$$

Here $J(M,I)$ is the $M \leftrightarrow M-1$ transition probability and τ is the interpulse delay of the solid-echo pulse sequence. In practice, however, the situation is not so complex because the width of satellite lines increases as M^2 and their intensity decreases, respectively, as $1/M^4$. In this case we can use a one-exponential approximation for the relaxation of magnetization of the two $\pm 3/2 \leftrightarrow \pm 1/2$ transitions, neglecting the contribution of other transitions. As can be seen from Fig. 6, the magnetization related to satellites really shows a one-exponential decay and the corresponding NMR line shape can be well fitted by a Lorentzian function [solid line in Fig. 4(a)].

From the consideration given above it is clear that the observed critical shortening of the spin-spin relaxation time at $T \rightarrow T_a^+$ is related to critical rotational fluctuations of the oxygen octahedra in agreement with results obtained by Müller *et al.*¹⁵ from the analysis of the temperature dependence of the EPR linewidth of the $\text{Fe}^{3+}\text{-V}_\text{O}$ pair center. However, in contrast to the EPR measurements, where the local fluctuations are entirely static at $T \rightarrow T_a^+$ on the time scale of the EPR technique, in the case of NMR the local-rotation fluctuations are essentially dynamic. From the motional narrowing condition $\tau_{\text{exch}}^{-1} \geq \tau_{\text{NMR}}^{-1} \approx \sqrt{M_2} = \nu_q$ one can estimate the lower limit of the characteristic frequency of the local rotation fluctuations at T_a . Taking the mean value of the rotation angle $\langle \phi^2 \rangle^{1/2} = 0.3^\circ - 0.4^\circ$ near T_a (Ref. 15) and, respectively, $\nu_q = 5-6$ kHz we obtain $6 \text{ MHz} > \tau_{\text{exch}}^{-1} > 6 \text{ kHz}$. The upper limit, about 6 MHz is found from EPR experiments.

It should be noted that ^{47}Ti and ^{49}Ti NMR measurements in STO-16 and STO-18 have also revealed⁸ that dynamic disorder of Ti ions coexists with the displacive soft mode. The Ti ions are off-center in the cubic phase and perform biased jumping between eight equilibrium sites located on the body diagonals. In addition, small and randomly oriented “tetragonal” nanoclusters exist already in the cubic phase. These nanoclusters correspond to different biasing of the occupations of the Ti sites and are responsible for the dynamic distortion of the oxygen frame and the small, yet nonzero quadrupole coupling in the cubic phase above T_a . The nonzero quadrupole coupling and its time fluctuations result in a smearing-out of the first-order satellites in the cubic phase, giving rise to the broad background component instead of sharp lines. The sharp central line seen in the ^{47}Ti , ^{49}Ti , and ^{87}Sr spectra, on the other hand, is due to the $1/2 \leftrightarrow -1/2$

transition which is not affected by the quadrupole coupling in first order.

C. ^{87}Sr NMR spectra in the low-temperature noncubic phase

The central $1/2 \leftrightarrow -1/2$ transition is affected by quadrupole coupling only in second order. We already mentioned that at the orientation $\mathbf{B} \parallel [110]$ the NMR line splits into two components below T_a [Fig. 5(a)]. In the general case of a multidomain state a splitting of the ^{87}Sr NMR line into three components is anticipated in the tetragonal phase. However, for $\mathbf{B} \parallel [110]$, two of the lines have matching resonance frequencies since $\Theta = 45^\circ$ for the $[100]$ and $[010]$ domains. For the third, $[001]$ domain, $\Theta = 90^\circ$.

The frequency shift of the ^{87}Sr $1/2 \leftrightarrow -1/2$ NMR line depends on both the quadrupole coupling and screening of the external magnetic field by the electron cloud (chemical shift):

$$\Delta\nu_{1/2 \leftrightarrow -1/2} = \Delta\nu_{1/2 \leftrightarrow -1/2}^{(2)} + \nu_L [1 + \delta_{iso} + \delta_{ax}(3 \cos^2 \theta - 1)], \quad (17)$$

where

$$\delta_{iso} = \frac{1}{3}(\delta_1 + \delta_2 + \delta_3), \quad \delta_{ax} = \frac{1}{6}(2\delta_3 - \delta_2 - \delta_1), \quad (18)$$

and δ_1 , δ_2 , and δ_3 are the three principal values of the chemical shift tensor δ ; for the cylindrical symmetry $\delta_1 \equiv \delta_2$. Equation (17) thus allows one to calculate both the quadrupole frequency ν_q and the chemical shift δ_{ax} using measured resonance frequencies at $\theta = 45^\circ$ and $\theta = 90^\circ$.

The temperature dependence of the ^{87}Sr quadrupole frequency ν_q so obtained in the tetragonal phase of STO is shown in Fig. 5(b). ν_q slowly increases with decreasing temperature and saturates at about 70 kHz below 30 K in STO-16. For STO-18, there are two slightly resolved components below 25 K [Fig. 5(a)]. The second component, which appears below 25 K, is related to a lowering of crystal symmetry. In STO-18 below 25 K, ν_q is slightly larger than in STO-16. On the other hand, the chemical shift is small ($\delta_{ax}\nu_L = 15\text{--}25$ Hz between 80 and 14 K) due to the low Larmor frequency of ^{87}Sr .

There is no domain splitting for $\mathbf{B} \parallel [111]$ as the ^{87}Sr NMR lines for all three domains coincide at this orientation, where $\Theta = \Theta_m = 54.7^\circ$. At this orientation there is also no influence of the ^{87}Sr chemical shift because $3 \cos^2 \Theta_m - 1 = 0$. The NMR shift should be therefore here proportional to the fourth power of the rotation angle ϕ , which is also the order parameter of the cubic to tetragonal transition. The temperature dependence of the $1/2 \leftrightarrow -1/2$ ^{87}Sr quadrupole shift is shown in Fig. 7. It should be mentioned⁹ that in addition to the main tetragonal line a second nontetragonal component appears below 70 K in STO-18. A similar component is seen also in STO-16 but its intensity (~ 5 to 6%) is much lower than in STO-18.⁹ Using the temperature dependence of the $1/2 \leftrightarrow -1/2$ ^{87}Sr NMR shift measured at $\mathbf{B} \parallel [111]$ we can check the functional dependence of the frequency shift (or, equivalently, ν_q) on the order parameter, i.e., the relation $\Delta\nu_{1/2 \leftrightarrow -1/2}(T) \propto \phi^4(T)$ [see Eqs. (1) and (10)] and determine the temperature dependence of the $\phi(T)$ using Fe^{3+} ESR data

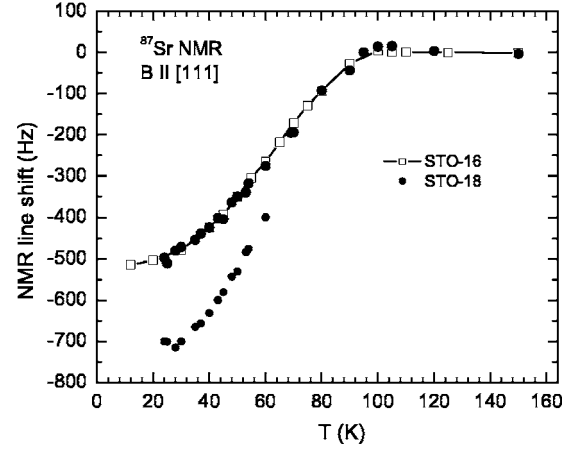


FIG. 7. Temperature dependence of ^{87}Sr NMR line shift at $\mathbf{B} \parallel [111]$ for STO-16 and STO-18.

as the reference. The comparison with the ESR data allows us to calculate the proportionality coefficient between ν_q and ϕ^2 which includes tunable parameters of the point charge model such as the antishielding factor and the effective charges of ions.

The temperature dependence of ϕ derived from the present NMR data is shown in Fig. 3 for both STO-16 and STO-18. For STO-16 the rotation angle varies between 0° and 2° in good agreement with the Fe^{3+} EPR data obtained with the same crystal. The temperature dependence of ϕ determined from the larger, i.e., tetragonal component of STO-18 agrees with the STO-16 data. This is, however, not the case for the nontetragonal component arising from rhombohedral clusters which start to form below 70 K as reported before.⁹ The data for STO-18 are shown only above 25 K as below this temperature the phase is no more tetragonal in the whole crystal. As we have already published,⁹ at these temperatures the NMR spectrum clearly demonstrates noncylindrical symmetry of the EFG tensor and the ^{87}Sr NMR line splits into three resolved or unresolved components depending on the domain structure. However, the angular dependence of the ^{87}Sr spectrum is still mainly determined by the large tetragonal components of the EFG tensor. The rhombohedral perturbation results in the small line splitting at $\mathbf{B} \parallel [111]$ and $\mathbf{B} \parallel [110]$. The symmetry of the new phase at $T < 25$ K is orthorhombic or monoclinic as the rhombohedral perturbation is superimposed on the tetragonal distortion of the cubic phase. Another interesting fact which should be noted is that the relatively narrow rhombohedral-symmetry lines “sit” on a broad background (see Fig. 3 of Ref. 9) which also appears at $T < 25$ K. This demonstrates the presence of a disordered glasslike component in the phase transition of STO-18. The amount of the disordered component is around 50%.

The observed lowering of the crystal symmetry of STO-18 leaves open the question if the corresponding atomic shifts are polar (related to possible ferroelectric phase transition) or nonpolar (some kind of antiferrodistortive transition with complex oxygen octahedron rotations). This can be checked by the application of an external electric field which has to redistribute the domain population along the electric

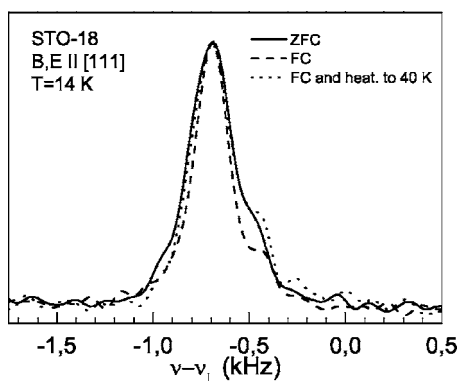


FIG. 8. FC and ZFC ^{87}Sr $1/2 \leftrightarrow -1/2$ NMR spectra of STO-18. The electric field ($E=50\text{--}150$ kV/m) was applied along $[111]$ at $T=30$ K. NMR spectra were measured at $T=14$ K after ZFC (solid line), FC from $T=30\text{--}14$ K (dashed line), and after subsequent heating of the FC sample to 40 K (dotted line).

field in the case of polar domains (or clusters) and does not change their population for unpolar domains.

The field cooled (FC) and zero field cooled (ZFC) ^{87}Sr NMR $1/2 \leftrightarrow -1/2$ spectra of STO-18 were measured for $\mathbf{E} \parallel \mathbf{B} \parallel [110]$ and $\mathbf{E} \parallel \mathbf{B} \parallel [111]$ and are shown in Fig. 8 for $\mathbf{E} \parallel \mathbf{B} \parallel [111]$ at $T=14$ K. Changes in the NMR line shape were observed for $\mathbf{E} \parallel \mathbf{B} \parallel [111]$ for electric fields exceeding $E=50$ kV/m, demonstrating that the rhombohedral clusters are polar and that we indeed deal with a ferroelectric multi-domain state. Note that the critical field for an electric field-induced ferroelectric phase transition¹⁹ in STO-16 is $E \approx 200$ kV/m. It should also be emphasized that application of the external electric field along the $[110]$ axes does not produce any visible change in the ^{87}Sr spectrum for field strengths up to 250 kV/m. Subsequent heating of the FC sample to 35–40 K (dotted line in Fig. 8) completely erases the effect of the electric field. No changes in the NMR line shape were observed with electric field at $T > 25$ K, i.e., at $T > T_c$. The effect of polarized electric field in STO-18 is rather small in comparison with that in ordinary ferroelectrics. This, however, agrees with a very small value of the electric polarization measured in STO-18 at $E \parallel [110]$ ($P_S = 0.3 \mu\text{C}/\text{cm}^2$, Ref. 3). To our knowledge, there were no measurements of polarization at $E \parallel [111]$, where in accordance with our result a larger value of the polarization can be expected. We cannot exclude that the $[111]$ cut thin plate contains predominantly 180° polar domains oriented along the $[111]$ axis, so that their reorientation in the electric field does not effect the NMR line shape because of the 180° symmetry of the NMR spectra. In any case, we have to no-

tice that the polarization in STO-18 is very small. This agrees with the relatively small changes in the crystal structure which are detected by ^{87}Sr quadrupole perturbed NMR and are hardly visible by $^{47,49}\text{Ti}$ NMR. The electric-field effect on the ^{87}Sr NMR spectrum thus supports the polar rhombohedral type perturbation of the tetragonal lattice of STO-18.

V. CONCLUDING REMARKS

The above results show that local symmetry breaking takes place also at the A-site of the “cubic” perovskite lattice and not only at the B-site as observed before.^{7,8} In the high temperature cubic phase local tetragonal-like clusters exist because of Ti ions being dynamically disordered between eight off-center sites, and the cubic symmetry is locally tetragonally broken. Local nontetragonal symmetry breaking takes place in the antiferrodistortive tetragonal phase below 70 K due to low symmetry clusters both in STO-18 and STO-16. These clusters percolate below $T_c \approx 24$ K in STO-18, leading to an inhomogeneous ferroelectric state.⁹ One should also mention that the relatively narrow ^{87}Sr NMR lines of the rhombohedral-symmetry spectrum sit on a broad background spectrum which appears below 25 K and demonstrates the presence of a disordered glasslike component in STO-18 below T_c .

It should be mentioned that noncentrosymmetric nanoregions with locally broken tetragonal symmetry have been observed²⁰ by second harmonic generation (SHG) microscopy in both STO-16 and STO-18. Whereas their concentration is T -independent in STO-16, it sharply increases on approaching T_c in STO-18.

It should be also noted that a rhombohedrally distorted polar state, where all components of the T_{1U} soft optic mode soften simultaneously, takes place in KTaO_3 doped with Li or Nb²¹ as well. Such a distortion would lead to a triclinic state in STO because of the superposition on the tetragonal distortion below T_a .

The fact that a ferroelectric transition occurs in STO-18 and not in STO-16 could be related to the different concentrations of the low symmetry clusters. In STO-18 the nanoclusters percolate at the ferroelectric transition at $T_c=24$ K, giving rise to a two-component state below T_c . In STO-16, the clusters’ concentration seems to be too small to allow for a percolation to take place. The interaction among clusters is clearly phonon-mediated and depends on the inverse square of the soft phonon frequency. This could explain the isotope effect, i.e., the replacement of ^{16}O with ^{18}O as the cluster-cluster interaction constant is in view of the lower frequency is larger in STO-18 than in STO-16.

¹J. F. Scott, Rev. Mod. Phys. **46**, 83 (1974).

²K. A. Müller and H. Burkard, Phys. Rev. B **19**, 3593 (1979); see also W. Zhong and D. Vanderbilt, *ibid.* **53**, 5047 (1996).

³M. Itoh, R. Wang, Y. Inaguma, T. Yamaguchi, Y. J. Shan, and T. Nakamura, Phys. Rev. Lett. **82**, 3540 (1999); R. Wang and M. Itoh, Phys. Rev. B **64**, 174104 (2001).

⁴K. A. Müller, W. Berlinger, and F. Waldner, Phys. Rev. Lett. **21**, 814 (1968); H. Unoki and T. Sakudo, J. Phys. Soc. Jpn. **23**, 546 (1967).

⁵K. A. Müller, W. Berlinger, and E. Tosatti, J. Phys. B **84**, 277 (1991).

⁶E. Pytte and J. Feder, Phys. Rev. B **1**, 4803 (1970).

- ⁷B. Zalar, V. V. Laguta, and R. Blinc, Phys. Rev. Lett. **90**, 037601 (2003).
- ⁸B. Zalar, A. Lebar, J. Seliger, R. Blinc, V. V. Laguta, and M. Itoh, Phys. Rev. B **71**, 064107 (2005).
- ⁹R. Blinc, B. Zalar, V. V. Laguta, and M. Itoh, Phys. Rev. Lett. **94**, 147601 (2005).
- ¹⁰R. Ernst, S. Bodenhausen, and A. Wokaun, in *Principles of NMR in One and Two Dimensions* (Oxford University Press, New York, 1987).
- ¹¹R. R. Hewitt, Phys. Rev. **121**, 45 (1961).
- ¹²F. Borsa, Phys. Rev. B **7**, 913 (1973).
- ¹³R. Sommer, M. Maglione, and J. J. van der Klink, Ferroelectrics **107**, 307 (1990).
- ¹⁴A. Abragam, in *Principles of Nuclear Magnetism* (Oxford University Press, New York, 1961).
- ¹⁵Th. von Waldkirch, K. A. Müller, and W. Berlinger, Phys. Rev. B **7**, 1052 (1973); G. F. Reiter, W. Berlinger, K. A. Müller, and P. Heller, *ibid.* **21**, 1 (1980).
- ¹⁶S. Geschwind, Phys. Rev. **121**, 363 (1961).
- ¹⁷S. A. Al'tshuler and B. M. Kozyrev, in *Electron Paramagnetic Resonance in Compounds of Transition Elements* (Wiley, New York, 1974).
- ¹⁸V. G. Grachev, *Programs Package Visual EPR*, University of Osnabrueck.
- ¹⁹J. Hemberger, P. Lunkenheimer, R. Viana, R. Böhmer, and A. Loidl, Phys. Rev. B **52**, 13159 (1995).
- ²⁰Y. Uesu, R. Nakai, J. M. Kiat, C. Menoret, M. Itoh, and T. Kyomen, J. Phys. Soc. Jpn. **73**, 1139 (2004).
- ²¹G. Kugel, H. Vogt, W. Kress, and D. Rytz, Phys. Rev. B **30**, 985 (1984).